Infusion of a Semidilute Bimodal Polymer Solution into Small Pores: Partitioning Inversion and Oscillatory Behavior

Anil Dube and Iwao Teraoka*

Department of Chemical Engineering, Chemistry, and Materials Science, Polytechnic University, 333 Jay Street, Brooklyn, New York 11201

Received May 7, 1997; Revised Manuscript Received October 3, 1997[⊗]

ABSTRACT: When a semidilute polymer solution is equilibrated with a porous medium filled with solvent, the high osmotic pressure due mostly to high molar mass components (HMC) drives low molar mass components (LMC) preferentially into the pores. Infusion transients of solvated polystyrene into a confined space of a porous medium from a free external solution were studied for an equal mass mixture of two polystyrene standards at several concentrations higher than the overlap concentration. The total pore volume was almost equal to the volume of the surrounding solution. Initially, both components, especially LMC, filled the pores until their concentrations became excessively high. Thus, the exterior solution was depleted in LMC; i.e., the partitioning was inverted for LMC, but enrichment of LMC in the pore was small. Subsequently, both components decreased the concentrations in the pores. The approach to the equilibria after the rapid infusion was slow and accompanied by an oscillatory pattern, especially evident for HMC. We explain the phenomenon as the one caused by coupling of the chain contraction of HMC due to overcrowded LMC in the pores and a large difference in the diffusivity between the two components.

Introduction

Partitioning of solvated polymers into a confined pore space of porous material underlies gel permeation chromatography (GPC).[1−3] At low concentrations each polymer molecule interacts with the pore independently. A decrease in the conformational entropy by the pore is an increasing function of the molar mass of the polymer.[1,4−6] Larger molecules are more strictly excluded by the stationary phase and elute earlier. At high concentrations, however, repulsions between solvated molecules surpass the free energy of confinement. The high osmotic pressure of the solution forces the polymer to enter the pores in a greater proportion. The partition coefficient, defined as the ratio of the concentration in the pores to that in the surrounding solution, approaches unity at sufficiently high concentrations. The weak-to-strong penetration transition was predicted by the scaling theory[7,8] and confirmed by experiments[9,10] as well as by computer simulations.[11,12]

When the polymer is polydisperse, the osmotic pressure-driven migration favors low molar mass components. The partition coefficient for these components exceed unity (i.e., the partitioning is inverted), whereas the coefficients for the other components remain low. Enhanced partitioning fractionation (EPF) was introduced to take advantage of the segregation with respect to the molar mass.[13,14] EPF consists of two steps. In step 1, a concentrated solution of the polydisperse polymer is equilibrated with a solvent-imbibed porous material. The high osmotic pressure due mostly to high molar mass components drives preferentially low molar mass components into pore channels. The exterior solution deficient in low molar mass components is physically separated to recover a fraction enriched with high molar mass components. Subsequently, low molar mass components in the pores are driven out by immersing the porous material into the pure solvent. The exterior solution is again physically separated to recover a fraction enriched with low molar mass components. We applied EPF to a solution of an equal mass mixture of two polystyrene standards and investigated how the pore size in spherical porous glass beads of diameter of about 2 mm, the molar mass of the polymer, and the processing time affect the performance of EPF.[15] EPF was later transformed into high osmotic pressure chromatography that realizes EPF at every plate as the polymer is transferred along the column.[16−18]

We recently applied space-resolved Jamin interferometry to the studies of the infusion of monodisperse polystyrene into a solvent-imbibed porous glass bead of diameter of about 2 mm.[19] There was a component that entered and permeated the porous medium immediately after adding the polymer to the surrounding solution. Subsequently, other polymer molecules infused into the medium to settle at an equilibrium concentration. When the average dimension of the polymer was greater than the pore size, entrance into the pores was rate-limiting. For shorter chains, in contrast, the entrance was easier compared with the permeation and the overall rate of infusion was faster.

In this paper we study infusion of a bimodal polymer solution into the pores of controlled pore glasses of size of about 0.15 mm. We interrupted EPF at various periods of time to find the compositions and the amounts of the polymers in the interior of the porous materials and in the surrounding solution, as the system approached the concentration equilibrium. In this way, the infusion of each component was traced as a function of time for different initial concentrations. In addition to the partitioning inversion, there was an oscillatory manner in which the system approached the equilibrium. We will explain the observed time dependence in terms of fluxes of the two components caused by a large difference in the chemical potential between the solution in the pore and the surrounding solution. The partitionings of the two components are highly coupled.

Experimental Section

Polymer Samples. Polystyrene (PS) standards were purchased from Pressure Chemical. Table 1 lists their characterization data. The radii of gyration, R_{g0}, in the dilute solution limit were calculated from the literature.[20] The

[⊗] Abstract published in *Advance ACS Abstracts,* December 1, 1997.

S0024-9297(97)00643-8 CCC: $14.00

Table 1. Characterization of Polystyrene Standards

sample	peak molar mass	polydispersity	R_{g0}, nm	c^*, mg/mL
PS30K	30 300	1.06	5.8	91.2
PS90K	89 300	1.04	11.1	39.4
PS288K	293 000	1.06	22.2	15.3
PS949K	949 000	1.06	44.8	6.12

overlap concentration c^* is defined as $c^*(\sqrt{2}R_{g0})^3 = M/N_A$, where M is the molar mass and N_A is Avogadro's number.

Porous Glasses. Controlled pore glass (CPG) is a gift from CPG, Inc. The average pore diameter is 15.6 nm, the pore volume is 0.81 cm^3/g, and the surface area is 90.9 m^2/g. The particle size is 80/120 mesh (~150 μm). Surface silanol groups were replaced by trimethylsilanyl groups to prevent adsorption of polymer. CPG were first soaked in concentrated nitric acid at 90 °C and then in hydrochloric acid at room temperature. The CPG was washed in water until neutral. After being dried, CPG was silanized by 2 M chlorotrimethylsilane in toluene under nitrogen at 90 °C for 2−4 days.

Enhanced Partitioning Fractionation. Original bimodal PS solutions were prepared by dissolving two PS standards of an equal mass in toluene. The total concentration ranged from 2 to 15 wt %. Surface-treated CPG was held in an open-end glass tube with a diameter of about 13 mm and a length of about 4 cm. A fluoropolymer screen of mesh size ~70 μm (Spectrum) was attached to one of the ends of the tube to retain the porous material. The CPG in the tube was first soaked in excess toluene in a vial. Air trapped inside the packed bed of CPG was removed in vacuum for about 1 min. Then nitrogen was blown from the open end of the tube for about 3 s to remove the interstitial toluene. Care was taken to retain the solvent in the pore channels. Then the original bimodal PS solution of a volume nearly equal to the total pore volume of the CPG was added from the open end of the tube by using a pipette. The tube was enclosed in a shell vial of diameter 21 mm with a polyethylene cap. There was always a solution between the inner wall of the vial and the outer wall of the tube. The vial was then placed on a rotation stage. For a processing time that exceeded 24 h, the polyethylene cap was wrapped with Al foil to prevent absorption of the solvent. Evaporation was minimized by placing the vial in a large glass jar that had an extra open vial containing a small amount of toluene to saturate the atmosphere with vapor. A loss of solvent from the solution was monitored by a change in the mass of the shell vial. The average change of the mass of the total liquid in a shell vial was within 1−2%. Typically, 0.6−1.7 g of the porous material and 0.6−1.0 mL of the PS solution were used. The ratio of the volume of the original polymer solution to the total pore volume was 1.1−1.2.

As explained earlier, EPF consists of two main steps, but we recovered fractions in four parts to increase the accuracy in the measurement of the compositions and the amounts of polymer in the solution in the pores and in the surrounding solution. At the end of step 1, the external solution was separated by blowing nitrogen from the open end of the tube for about 5 s to extrude the interstitial solution as fraction 1. Then the CPG in the tube was soaked in toluene in another vial, and within 40 s the interstitial fluid was similarly removed as fraction 2. In step 2 of EPF, the tube was transferred to another shell vial, and excess toluene was added to drive out the polymer from the pores. After 1 day the surrounding solution was separated as fraction 3. Subsequently, toluene was added to the CPG in another vial. After 1 day the external solution was separated to recover fraction 4. All of the processing was carried out at room temperature. Polystyrene was precipitated from each solution by adding excess methanol. The polymer in each fraction was dried in a vacuum oven at 40−60 °C overnight before weighing. Nearly all of the polymer in the original solution was recovered in the four fractions. Molar mass distributions of the four fractions and the original mixture were analyzed in tetrahydrofuran by using a Waters GPC system with a Model 510 pump, a Model 410 differential refractometer, and a single size-exclusion column (American Standards, 10^6 Å pore).

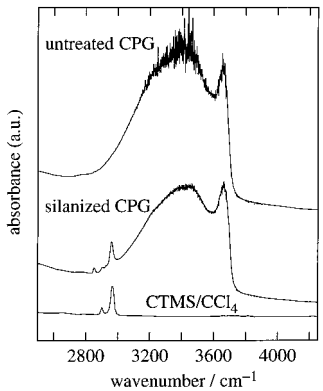

Figure 1. FTIR spectra of untreated CPG, silanized CPG, and a solution of CTMS in CCl_4.

FTIR Analysis of Surface Treatment. We evaluated the surface modification of CPG by using a Perkin Elmer 1600 series Fourier transform infrared spectroscopy (FTIR) system at wavenumbers ≥ 2500 cm^{-1}. The CPG was filled to ca. $^3/_4$ of an IR-grade silica cell with 1 mm path length (NSG, Type 1). Excess carbon tetrachloride (CCl_4) was introduced into the cell. Index matching (not exact) of CCl_4 to silica in the relevant range of wavenumber and the absence of hydrogen atoms facilitated the measurement of IR absorption spectra of moieties on the silica surface. Air trapped in the packed bed of CPG was removed by placing the cell in vacuum. A silica cell with CCl_4 was used as a background. Figure 1 shows the spectra of untreated CPG and silanized CPG. A broad peak at around 3400 cm^{-1}, present in both samples, is ascribed to hydroxyl groups in bulk silica. The spectrum of the treated sample has an additional peak at 2960 cm^{-1}, ascribed to the asymmetric C−H stretching in trimethylsilanyl moieties. For reference, an FTIR spectrum of chlorotrimethylsilane (CTMS) in CCl_4 was measured at several concentrations from 0.1 to 0.25 M. In Figure 1 is also shown the spectrum of the 0.25 M CTMS solution. A plot of the peak area (2960 cm^{-1}) as a function of the CTMS concentration produced a straight line. Its slope was used to estimate the CTMS−equivalent concentration of trimethylsilanyl attached to the surface of CPG as 0.39 M in the packed bed.

To convert this estimate to the number density of trimethylsilanyl on the surface, we measured the packing density of CPG in CCl_4. Measurement of a change in the height of a packed bed of CPG as more CPG was introduced into a glass tube of a given inner diameter led to the estimate of the packing density as 4.47×10^{-1} g/cm^3. With the specific surface area of 90.9 m^2/g, the surface area of the packed bed was estimated to be 40.6 m^2/cm^3. The number of trimethylsilanyl groups per unit surface area of CPG was then calculated as 9.6 $\mu M/m^2$ or 5.8 nm^{-2}.

In a separate experiment, we characterized the surface of silanized silica gels (150 Å, 100/200 mesh, W. R. Grace). The CTMS−equivalent concentration of trimethylsilanyl attached to the surface was estimated as 0.26 M. We estimated the packing density and the surface area per unit volume as 3.49×10^{-1} g/cm^3 and 115 m^2/cm^3, respectively. Thus, the number of trimethylsilanyl groups per unit surface area was calculated as 1.4 nm^{-2}, in agreement with the reported value of 3 $\mu M/m^2$ or 1.8 nm^{-2}.[21]

Results

The results shown below were obtained for equal mass mixtures of PS949K and PS90K unless otherwise mentioned. Figure 2 shows an example of GPC chromatograms for the original bimodal polystyrene solution with c_{tot} = 11.3 wt % and four fractions obtained in EPF, where c_{tot} is the total concentration in the original solution. The two peaks are well separated to allow us to calculate the area under each peak that is proportional to the mass of each component. The period T_1 for step 1 was 3 h. In fraction 1, the high molar mass

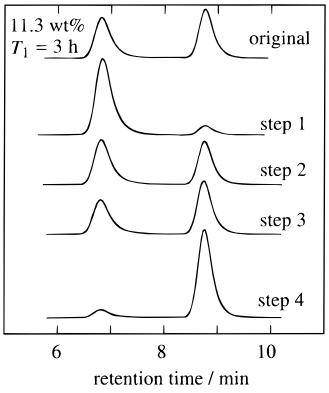

Figure 2. GPC elution curves of EPF products obtained for an equal mass mixture of polystyrene standards of M_p = 949 000 and 89 300 at a concentration of 11.3 wt %. Step 1 product was recovered in 3 h.

component (PS949K; HMC) was enriched to 90.6% by mass. Similarly, there is enrichment of the low molar mass component (PS90K; LMC) in fraction 3 with a mass fraction of 0.640. Fraction 2 had a purity between those of fractions 1 and 3. Fraction 4 usually had a mass fraction of LMC greater than that of fraction 3, but the amount was smaller. Afterward, fraction 4 was combined with fraction 3. The combined fraction is considered to have the composition of the polymer in the pores at the end of step 1. Fraction 1 is expected to represent the composition of the solution exterior to the pores. Fraction 2 consists of the exterior solution that sticks to the bead surface and the solution in the pores near the surface. We therefore divided the mass of fraction 2 into two parts that have the compositions of fractions 1 and 3.

We denote by m_{HI} and m_{LI} the masses of HMC and LMC, respectively, in the pore channels in time T_1 after the original solution was added. Likewise we define m_{HE} and m_{LE} for the exterior solution. Our interest is in purity p_{HE} of HMC in the exterior solution and purity p_{LI} of LMC in the solution in the pores. They are defined as

$$p_{HE} \equiv m_{HE}/(m_{HE} + m_{LE}), \qquad p_{LI} \equiv m_{LI}/(m_{HI} + m_{LI}) \tag{1}$$

We are also interested in the partition coefficients K_H and K_L of HMC and LMC defined as

$$K_H \equiv c_{HI}/c_{HE}, \qquad K_L \equiv c_{LI}/c_{LE} \tag{2}$$

where c_{HI} and c_{HE} are the concentrations of HMC in the pores and in the exterior solution, respectively. Similarly, c_{LI} and c_{LE} are the concentrations of LMC in the pores and in the exterior solution, respectively. The purities were calculated from the compositions of fractions 1 and 3. The weight concentrations were estimated from the compositions and masses of fractions 1−3. Although the partitioning is an equilibrium phenomenon, we use K_H and K_L also for transients.

Figure 3 shows K_H and K_L as a function of T_1 for c_{tot} = 5.3, 7.8, 9.8, and 11.3 wt %. We find some common features independent of c_{tot}. First, infusion of polymers into the solvent-filled pores was rapid. A large amount of polymer was driven into the pores even for $T_1 \cong 0.4$ h. Experimental difficulties prevented measurements at a shorter T_1. Second, $K_L > K_H$ and $K_L > 1$ always held. The shorter chains were more easily accommodated by the pores. K_H was surprisingly large. K_H

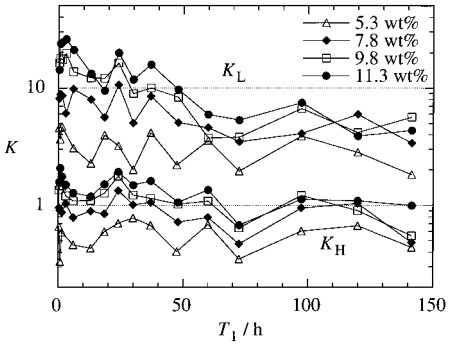

Figure 3. Partition coefficients K_H and K_L of the high and low molar mass components plotted as a function of time T_1 for four concentrations of PS949K/PS90K in the original solution.

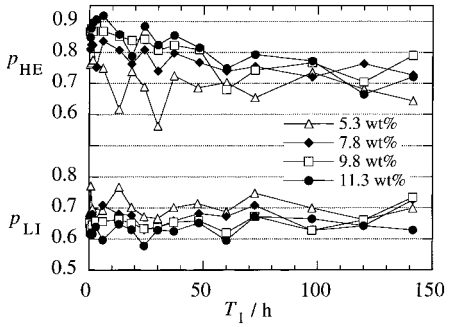

Figure 4. Purities p_{HE} and p_{LI} of the exterior solution and the solution in the pores, respectively, shown as a function of time T_1 for four concentrations of PS949K/PS90K in the original solution.

exceeded unity at short T_1 for c_{tot} = 9.8 and 11.3 wt %. Third, there appears to be some periodicity in the time dependence, especially for K_H. The plots resemble a damped oscillation. The period does not appear to depend on c_{tot}. Fourth, there is a long-time decreasing trend in K_H and K_L, especially for a higher c_{tot}, superimposed on the oscillatory behavior. Over a long time, K_H approached a value less than unity. There are also features that depend on c_{tot}. Compared at the same T_1, both K_H and K_L tended to be greater for a higher c_{tot}. For c_{tot} = 11.3 wt %, K_L exceeded 30 at T_1 = 6 h. The difference among the four values of c_{tot} was evident for $T_1 < 50$ h but later became less pronounced. Decreases in K_H and K_L, especially in K_L, over time were greater for a higher c_{tot}. The concentration dependencies of K_H and K_L are in agreement with the predictions.[14]

Figure 4 shows the purities p_{HE} and p_{LI} as a function of T_1. The original unfractionated solutions have a purity of 0.5. p_{LI} remained almost unchanged. There is a decreasing trend for p_{HE}, especially at a higher c_{tot}. Initially, a large proportion of polymer chains infused into the pores as seen in Figure 3. Most of the chains were LMC with p_{LI} between 0.6 and 0.7. Infusion continued until the exterior solution became deficient in LMC (large K_L), thereby producing a large p_{HE}. Subsequently LMC exuded from the pores, as seen in a decrease in K_L in Figure 3, depressing p_{HE} at longer times. At c_{tot} = 5.3 wt %, a variation in purity with time was present for both solutions, but there was no discernible long-time trend.

Also observed is a reverse effect of c_{tot} on p_{LI} and p_{HE}. Compared at the same T_1, p_{LI} was smaller for a higher c_{tot}, but p_{HE} was larger. At c_{tot} = 11.3% for $T_1 < 5$ h, a large K_L left the external solution enriched with HMC ($p_{HE} > 0.90$). At c_{tot} = 5.3 wt % in contrast, K_L was as

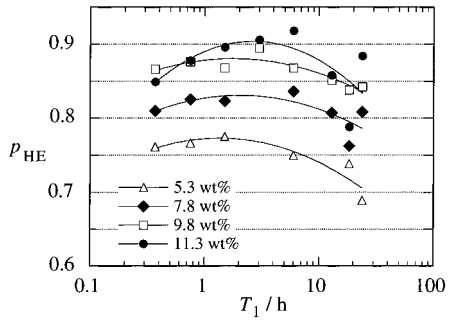

Figure 5. Purity p_{HE} is shown as a function of time T_1 for short periods only, for the four concentrations of the original solution.

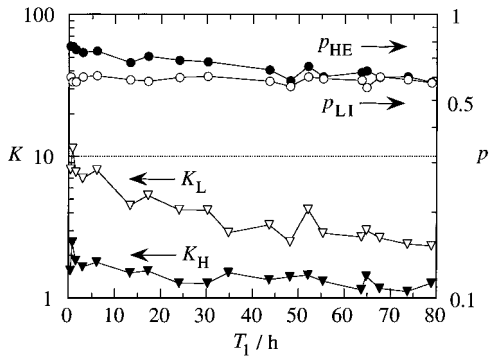

Figure 6. Partition coefficients K_H and K_L and purities p_{HE} and p_{LI} plotted as a function time T_1 for a 15 wt % original solution of PS288K/PS30K.

small as 2 with about 35% of LMC still remaining in the exterior solution to depress p_{HE} to 0.65. A solution of a lower c_{tot} has a weaker driving force to infuse polymer chains into the solvent-filled pores. Then the size exclusion dominates, resulting in a large p_{LI}, as predicted by calculations.[14] At long times, p_{HE} was the largest for c_{tot} between 8 and 10 wt %, whereas the lower concentration increased p_{LI}.

Figure 5 shows p_{HE} at short times. Peaking in p_{HE} occurred in 1−10 h. A higher c_{tot} shifted the peak toward a longer T_1. The shift is ascribed to a slower entrance of entangled polymer chains into the pores at higher concentrations. The best way to realize the largest p_{HE} is to equilibrate the porous medium with a solution of a high concentration and to terminate step 1 quickly.

We also performed infusion experiments up to 24 h for the PS949K/PS90K mixture at $c_{tot} = 2.0$ wt % using the same CPG. During the period, p_{HE} was held unchanged at around 0.55 and p_{LI} fluctuated between 0.57 and 0.63. K_L and K_H were around 1.0 and 0.5, respectively. There appears to be a periodic pattern in K_L and K_H, although the period was shorter than the one observed for samples at higher c_{tot}. Compared with EPF at higher concentrations, K_L is smaller and closer to K_H and p_{LI} and p_{HE} are smaller, in agreement with predictions.[14]

We conducted a similar experiment using an equal mass mixture of PS288K and PS30K and the same CPG. Figure 6 shows the partition coefficients and purities of HMC (PS288K) and LMC (PS30) as a function of T_1. In terms of the reduced concentration c/c^*, $c_{tot} = 15.0$ wt % for the mixture is similar to $c_{tot} = 5.3$ wt % for PS949K/PS90K. As was the case for PS949K/PS90K, K_L was larger than K_H and p_{HE} was higher than p_{LI}. Both K_L and K_H decreased slowly with time. Pseudo-periodic variations in K_L and K_H were absent. K_H exceeded unity at $T_1 \cong 80$ h. We expect that eventually K_H will become smaller than unity. p_{HE} also followed an overall decreasing trend, but p_{LI} remained almost constant, as was the case for PS949K/PS90K. The values of p_{HE} and p_{LI} were smaller compared with those of PS949K/PS90K. The pores do not provide PS288K/PS30K with geometrical restrictions sufficient to selectively admit LMC. Infusion was more rapid than that for PS949K/90K.

Among various characteristics in the changes of K_L, K_H, p_{HE}, and p_{LI} as a function of time, the concentration dependence is in agreement with theoretical predictions.[14] The greater the osmotic pressure, the more of LMC is forced to enter the pores, thus increasing p_{HE} and K_L. At the same time, the fraction of HMC forced to enter the pores is somewhat larger and p_{LI} decreases. There are two features that at first may appear inexplicable: (1) Why is there an oscillatory behavior? (2) Why is K_H so high at short times?

In the following section, we discuss, for a bimodal polymer solution, the difference in the chemical potential for each component between the solution in the pore and the exterior solution. A map of the chemical potentials as a function of K_L and K_H allows us to find the fluxes of the two components into the pores when the system approaches equilibrium.

Discussion

An infusion flux j_i (i = H and L for HMC and LMC, respectively) is defined as the mass of component i that enters the pores from the exterior solution per unit time per unit area of the pore openings on the surface of the glass bead. It is given by

$$j_i = \frac{V_I}{S}\frac{\partial c_{iI}}{\partial t} \quad (i = \mathrm{H, L}) \tag{3}$$

where V_I is the total pore volume and S is the total area of the openings on the porous glass bead. The driving force of the mass transfer is the difference in the chemical potential $\Delta\mu_i \equiv \mu_{iE} - \mu_{iI}$, where μ_{iE} is the chemical potential of component i in the exterior solution and μ_{iI} is defined for the solutions in the pores. We expect that j_i is an increasing function of $\Delta\mu_i$ and, for small differences in the chemical potentials, is written as

$$j_i = \alpha_i \Delta\mu_i \tag{4}$$

At near equilibrium, $\alpha_i = D_i c_{iS}$, where c_{iS} is the concentration of i at the bead surface and the diffusion coefficient D_i is taken at the surface.

Since $\Delta\mu_H$ and $\Delta\mu_L$ are functions of c_{HI} and c_{LI}, eqs 3 and 4 constitute a dynamical system.[22] The equilibrium is given by $\Delta\mu_H = \Delta\mu_L = 0$. Near the equilibrium, $\Delta\mu_i$ is given by a bilinear equation of differences of c_{HI} and c_{LI} from their respective equilibrium values. Relative magnitudes and signs of the linear coefficients determine how the system that consists of the interior solution and the exterior solution approaches equilibrium.

To see the behavior of c_{HI} and c_{LI} for a system near and far from the equilibrium, we calculated $\Delta\mu_H$ and $\Delta\mu_L$ as a function of K_H and K_L (or c_{HI} and c_{LI}) in wide ranges. The volume of the exterior solution was assumed to be equal to V_I. The solution before being forced to equilibrate with the solvent-filled porous medium is an equal mass mixture of the two components at concentrations c_{H0} and c_{L0}. Chain dimensions

of $R_{gH}/R_p = 1$ and $R_{gL}/R_p = 0.25$ were used. These chains are much smaller than PS949K and PS90K that have $R_{gH}/R_p = 6.0$ and $R_{gL}/R_p = 1.5$. Use of smaller chain dimensions narrowed the ranges of K_H and K_L needed for the calculation without changing the characteristics of the chemical potential differences. The osmotic pressure of a polymer solution was assumed to follow the interpolation formula derived by Ohta and Oono.[23] The confinement entropy of a polymer chain was assumed to be equal to that of a Gaussian chain with the same radius of gyration at a given concentration in the pore. The chain contraction factor used is the one derived also by Ohta and Oono.[23]

Parts a−c of Figure 7 are contour plots of $\Delta\mu_H/k_BT$ (solid line) and $\Delta\mu_L/k_BT$ (dashed line) as a function of K_H and K_L for the concentrations of the original solutions of c_{0H}/c_H^* and $c_{0L}/c_L^* = 0.115$ and 0.0189, 1.15 and 0.189, and 5.73 and 0.860, respectively. Values of c_{HI} and c_{LI} are indicated adjacent to K_H and K_L, respectively. The value of the chemical potential is indicated on each isopleth. The isopleths for $\Delta\mu_H = 0$ and $\Delta\mu_L = 0$ are drawn in thick lines. Their intersection ($K_{H,eq}$ and $K_{L,eq}$), indicated by a dot, represents the equilibrium. In Figure 7a, the isopleths for $\Delta\mu_H/k_BT$ are nearly perpendicular to the K_H axis and those for $\Delta\mu_L/k_BT$ are nearly perpendicular to the K_L axis. Equivalently, equilibration of each component is independent of the other component. Directions of fluxes that accrue (see eq 4; a positive j_i increases K_i) are obvious. In the quadrant of $K_H < K_{H,eq}$ and $K_L < K_{L,eq}$, for example, the resultant fluxes increase both K_H and K_L (c_{HI} and c_{LI}). Thus, if the system is away from the equilibrium, the fluxes let the system approach the equilibrium without traversing into other quadrants.

In Figure 7b, the isopleths are distorted. As more HMC is present in the pore, infusion of LMC becomes increasingly difficult. Thus, the isopleths for $\Delta\mu_L$ are bent left at a high K_H compared with nearly vertical lines in Figure 7a. The presence of LMC in the pore at a low K_L places only a low barrier against infusion of HMC. At a higher K_L the chain contraction of HMC due to shielding of the excluded-volume effect contributes to reduction of the entropic penalty, thereby facilitating the infusion. Thus, the isopleths for $\Delta\mu_H$ are not horizontal but show a dip, followed by an upturn, as K_L further increases to repel HMC out of the pores. Compared with Figure 7a, the equilibrium point has moved up and right. A large increase in $K_{L,eq}$ results in a value greater than unity (partitioning inversion). Note that the zero−$\Delta\mu_H$ isopleth is not horizontal and the zero−$\Delta\mu_L$ isopleth is not vertical in the neighborhood of the equilibrium point. Starting with the initial condition $K_H = K_L = 0$, the system will approach equilibrium, swirling around the equilibrium point counterclockwise. Taking into account that $D_H \ll D_L$, we find that the trajectory is elliptic, with its long axis nearly parallel to the K_L axis.

A stronger coupling of the partitioning of the two components at a higher concentration distorts the isopleths further, as shown in Figure 7c. The equilibrium point has moved further up and right. The partitioning is governed mostly by HMC, with the isopleths close to those of $\Delta\mu_H = 0$ and $\Delta\mu_L = 0$ running nearly parallel to the K_L axis. The zero−$\Delta\mu_H$ isopleth and the zero−$\Delta\mu_L$ isopleth are close to each other. The driving force that brings the system closer to the equilibrium point is weak once the system is near the two lines. Equivalently, there is a wide range of near-

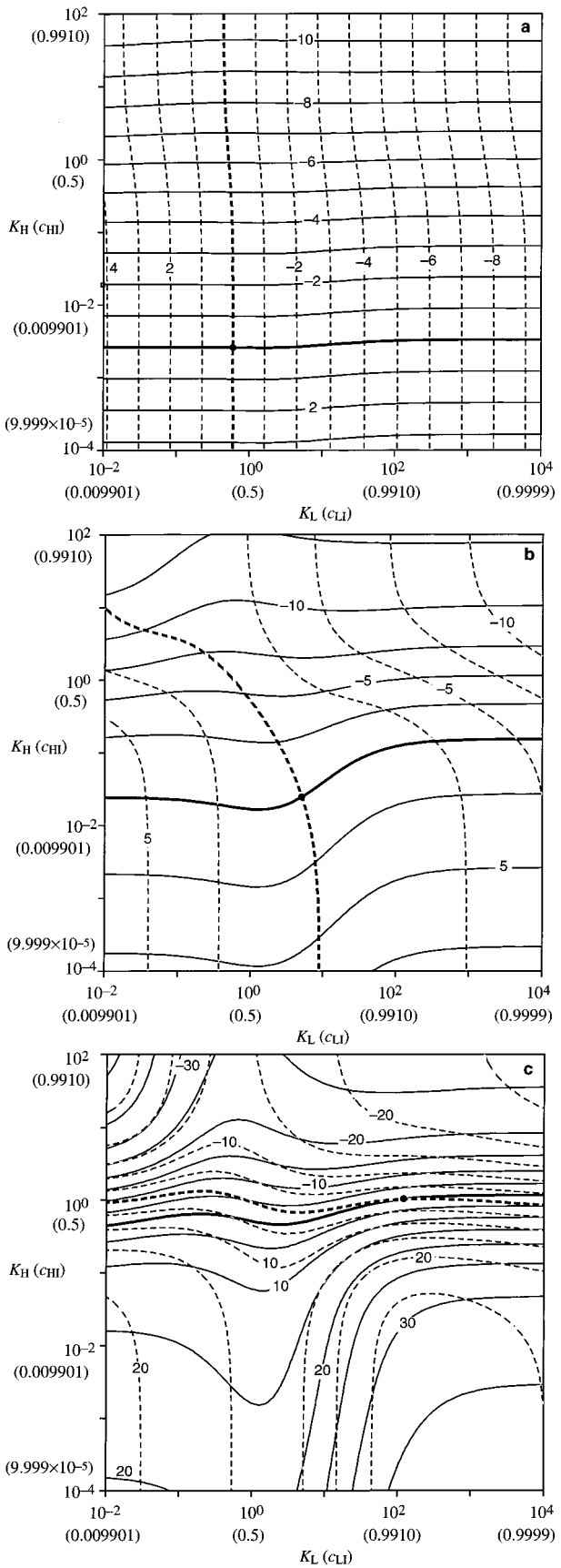

Figure 7. Isopleths of the chemical potential differences $\Delta\mu_H/k_BT$ (solid lines) and $\Delta\mu_L/k_BT$ (dashed lines) plotted as a function of K_H and K_L for the concentrations of the original solutions of c_{0H}/c_H^* and $c_{0L}/c_L^* =$ (a) 0.115 and 0.0189, (b) 1.15 and 0.189, and (c) 5.73 and 0.860. The isopleths for $\Delta\mu_H = 0$ and $\Delta\mu_L = 0$ are drawn in thick lines. The values of the differences are indicated on the lines.

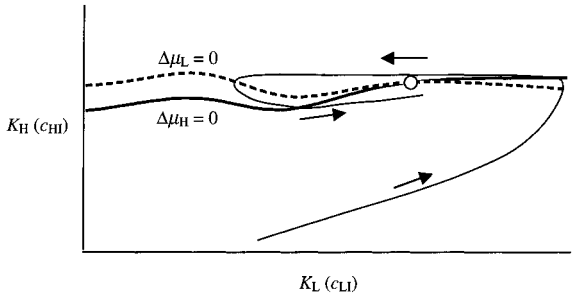

Figure 8. Expected path to approach equilibrium for a system given by Figure 7c.

equilibrium states. Below these lines, $\Delta\mu_H$ and $\Delta\mu_L$ are both positive, and they are negative above these lines. The vectors of the resultant fluxes point up and right below the lines and down and left above the lines (not shown). A large difference in the diffusivity between the two components makes the vectors nearly horizontal. In the quadrant of a narrow strip to the right of the equilibrium point, the vector is oriented up and left. In the other narrow strip to the left of the point, the direction is down and right. Note also that the isopleth for $\Delta\mu_L = 0$ is bent downward to the left of the equilibrium point. This curvature makes the approach to the equilibrium different from the one we saw in part a or b of Figure 7. The expected trajectory is shown in Figure 8. Starting with $K_H = K_L = 0$, the system will first cross the two lines on the right-hand side of the equilibrium point. Thus, there will be an overshoot in both K_H and K_L with $K_H \ll K_L$. Afterward, the system will move left on the map until it hits the isopleth of $\Delta\mu_L = 0$, then move down, and later right. The system may show an overshoot a few times before it finally reaches the equilibrium.

The overall pattern of the isopleths is almost identical at concentrations higher than the concentration in Figure 7c. The transition in the pattern from part a to c of Figure 7 is seen also for mixtures of longer chains that experience greater confinement effects. For mixtures of shorter chains, in contrast, the distortion in the isopleths is smaller, compared at the same reduced concentrations, c_{0H}/c_H^* and c_{0L}/c_L^*.

The behaviors of the flux directions and the trajectories are translated into physical phenomena as follows: At low concentrations, both HMC and LMC will infuse into the pores, with K_H and K_L increasing uniformly toward $K_{H,eq}$ and $K_{L,eq}$, respectively. There will be no oscillatory behavior as was found for PS949K/PS90K with $c_{tot} = 2.0$ wt %. At concentrations higher than the overlap concentration, the two components infuse into the pores initially to make the concentrations in the pore much higher than those at equilibrium. The high chemical potentials in the pore now decrease first the amount of LMC in the pore and then the amount of HMC. As the interior concentrations become too low, they again start to fill the pores. Thus, the infusion will be oscillatory, as we have seen in Figure 3. When the confinement is weak as in PS288K/PS30K, we will not see the oscillatory approach to equilibrium. In the actual system, the porous materials used have a finite particle size. The change in $\Delta\mu_i$ will cause the flux to change not instantaneously but rather with a delay.

Concluding Remarks

In the partitioning of a mixture of two polystyrene standards at high concentrations with a porous medium, we have shown that the partition coefficient for the low molar mass component is greater than unity, in agreement with the theoretical predictions. In short times, the exterior solution successfully removed the majority of low molar mass components. In high osmotic pressure chromatography, the mobile phase should be transferred to the next plate when the purity of HMC in the mobile phase hits the maximum. If the flow rate is too slow, the highly concentrated solution in the stationary phase will come out again to decrease the purity.

The map of the chemical potential differences indicated an oscillatory pattern in the approach of the solution−pore system to equilibrium. By tuning the chain dimensions, the pore size, and the concentrations, we may be able to construct a system that shows a pattern close to a limit cycle. The period will be determined by the ratios of the chain dimensions to the pore size. The experimental results shown here need to be reproduced in different mixtures of polymers and by other experimental techniques that can trace the change in the concentration of each component *in situ*.

Acknowledgment. Partial support by Petroleum Research Fund (American Chemical Society) and NSF Young Investigator Award is gratefully acknowledged. We also thank Dr. H. Wechsler for financial support.

References and Notes

(1) Giddings, J. C. *Unified Separation Science*; John Wiley: New York, 1991.
(2) *Chromatography of Polymers*; Provder, T., Ed.; American Chemical Society: Washington, DC, 1991; Vol. 521.
(3) Teraoka, I. *Prog. Polym. Sci.* **1996**, *21*, 89.
(4) Casassa, E. F. *J. Polym. Sci., Polym. Lett. Ed.* **1967**, *5*, 773.
(5) Giddings, J. C.; Kucera, E.; Russell, C. P.; Myers, M. N. *J. Phys. Chem.* **1968**, *72*, 4397.
(6) Casassa, E. F.; Tagami, Y. *Macromolecules* **1969**, *2*, 14.
(7) Daoud, M.; de Gennes, P.-G. *J. Phys. (Paris)* **1977**, *38*, 85.
(8) de Gennes, P.-G. *Scaling Concepts in Polymer Physics*; Cornell University Press: Ithaca, NY, 1979.
(9) Teraoka, I.; Langley, K. H.; Karasz, F. E. *Macromolecules* **1993**, *26*, 287.
(10) Teraoka, I. *Macromolecules* **1996**, *29*, 2430.
(11) Thompson, A. P.; Glandt, E. D. *Macromolecules* **1996**, *29*, 4314.
(12) Wang, Y.; Teraoka, I. *Macromolecules*, in press.
(13) Teraoka, I.; Zhou, Z.; Langley, K. H.; Karasz, F. E. *Macromolecules* **1993**, *26*, 3223.
(14) Teraoka, I.; Zhou, Z.; Langley, K. H.; Karasz, F. E. *Macromolecules* **1993**, *26*, 6081.
(15) Dube, A.; Teraoka, I. *Macromolecules* **1995**, *28*, 2592.
(16) Luo, M.; Teraoka, I. *Macromolecules* **1996**, *29*, 4226.
(17) Luo, M.; Teraoka, I. *Polymer*, in press.
(18) Teraoka, I.; Luo, M. *Trends Polym. Sci.* **1997**, *5*, 258.
(19) Dube, A.; Teraoka, I. *Macromolecules* **1997**, *30*, 5352.
(20) Huber, K.; Bantle, S.; Lutz, P.; Burchard, W. *Macromolecules* **1985**, *18*, 1461.
(21) Leyden, D. E. In *Silanes, Surfaces and Interfaces Symposium*; Gordon and Breach Science Publishers: Snowmass, CO, 1985.
(22) Nicolis, G.; Progogine, I. *Self-organization in non-equilibrium systems*; John Wiley: New York, 1977.
(23) Ohta, T.; Oono, Y. *Phys. Lett.* **1982**, *89A*, 460.

MA9706438